



Radio Science

RESEARCH ARTICLE

10.1029/2018RS006552

Key Points:

- Interferometric and high-speed video observations reveal the detailed discharge processes leading to large M component current pulses
- Large M events are caused by fast positive streamers followed by a possible recoil event or by a dart leader if an active channel exists
- M events with large peak currents occur shortly after a preceding return stroke, and their corresponding current changes are more rapid

Correspondence to:

Y. Zhang,
zhangyang@cma.gov.cn

Citation:

Zhang, Y., Zhang, Y. J., Zheng, D., & Lu, W. (2018). Characteristics and discharge processes of M events with large current in triggered lightning. *Radio Science*, 53, 974–985. <https://doi.org/10.1029/2018RS006552>


Received 16 FEB 2018

Accepted 19 JUL 2018

Accepted article online 3 AUG 2018

Published online 29 AUG 2018

Characteristics and Discharge Processes of M Events With Large Current in Triggered Lightning

Yang Zhang^{1,2} , Yi Jun Zhang^{1,3}, Dong Zheng^{1,2}, and Weitao Lu^{1,2}

¹State Key Laboratory of Severe Weather, Chinese Academy of Meteorological Sciences, Beijing, China, ²Laboratory of Lightning Physics and Protection Engineering, Chinese Academy of Meteorological Sciences, Beijing, China, ³Department of Atmospheric and Oceanic Sciences and Institute of Atmospheric Sciences, Fudan University, Shanghai, China

Abstract Observations have been obtained of M events during triggered lightning flashes with a broadband very high frequency interferometer and measurements of electric field changes, channel-base current, and high-speed video. The current characteristics of 239 M events in 18 triggered lightning flashes are analyzed, and the discharge processes leading to large M currents are investigated. Sixty-eight of the M events (28%) had peak currents exceeding 1 kA. The geometric average values of peak current, duration, 10–90% rise time, half peak width, charge transfer, interval from return stroke to M and background current are 2.358 kA, 0.627 ms, 0.078 ms, 0.165 ms, 0.417 C, 2.172 ms, and 579 A, respectively. Compared to other M events, the M events with large peak current occurred closer in time to the preceding return stroke, and their corresponding current changes were more rapid. Three cases associated with the initiation processes of M events reveal that some large M events were initiated by fast positive streamers propagating away at a velocity of about 10^7 m/s followed by a possible recoil event, or by a dart leader while the channel of continuing current generated by previous leader still existed. It is found that a fast current pulse with 10–90% rise time of less than 300 μ s is a necessary, but not sufficient, condition for the occurrence of large M events. The fast current pulse often corresponded to a low/close junction site.

Plain Language Summary As a typical charge transfer process during lightning discharge, most of M components are often associated with current pulse having a peak amplitude of 100–200 A and a charge transfer of 0.1 to 0.2 C. However, some large M components transfer as much charge as a return stroke and their peak currents may be up to several kiloamperes, which often cause severe damage. Although there was some research on large M components, the research mainly focused on charge transfer and current characteristics. Up to now, there is no widely accepted conclusion on the initiation of large M components. To better understand the formation cause of large M components, we thoroughly analyze the current characteristics of M components and the related discharge processes based on channel-base current data, high-speed video observations, and the radiation source locations of flash-continuous interferometer observations acquired from triggered lightning flashes. The study reveals that large M events are often caused by fast positive streamers followed by a possible recoil event or by a dart leader to ground if an active channel exists.

1. Introduction

As a typical charge transfer process during triggered lightning discharge, M components are often associated with transient perturbations in the relatively steady continuing current that follows return strokes (RSs), and enhance the channel luminosity (Rakov & Uman, 2003). Studies of M components often focus on current processes and luminous pulses in triggered lightning flashes (Qie et al., 2011, 2013; Rakov et al., 2001; Thottappillil et al., 1995; Wang et al., 2012) and in upward-initiated lightning flashes initiated from high buildings or towers (Flache et al., 2008; Wang et al., 2007; Zhou et al., 2015).

A typical M component during triggered lightning often produces a more or less symmetrical current pulse at the channel base. The current pulse has a peak amplitude of 100–200 A, a rise time of 300–500 μ s, and a charge transfer of 0.1 to 0.2 C (Fisher et al., 1993; Rakov & Uman, 2003; Thottappillil et al., 1995). The pulse is often viewed as the superposition of two guided waves which propagate in opposite directions from its initiation point inside the cloud (the so-called *two-wave* mechanism; Rakov et al., 1995). But some M components transfer as much charge as a RS and their peak currents may be up to several kiloamperes (Jiang et al.,

2011; Qie et al., 2011; Rakov, 1998; Wang et al., 2012). Large M components during RSs often cause severe damage due to their large current peak and charge transfer (Chen et al., 2018).

The discharge processes leading to large M components have rarely been quantitatively investigated in previous studies. The available research mainly focused on charge transfer and current characteristics of the M components. For example, Jiang et al. (2011) analyzed the characteristics of six large M components. They inferred that the M components develop from up to down and then contact to the ground, with the upward development continuing after contacting the ground. Subsequently, a modified two-wave mechanism was proposed that confirmed the evolution of M component as producing a downward wave transferring negative charge from the upper to the lower channel and an upward wave draining the charge transported by the downward wave (Jiang et al., 2013). Qie et al. (2011) presented observations of five large M components. The geometric means of the peak current, half peak width (HPW), and rise time from 10% to 90% peak were 5.1 kA, 76.3 μ s, and 34.6 μ s, respectively. They observed a special type of large M component called RM that exhibited both RS and M component features. It was proposed that RMs consist of the superposition of a dart leader and M incident wave in the channel. They speculated on the cause of RM type, but had no channel observations to support their claim.

Due to the difficulty of detecting and locating of in-cloud discharge, there are only a few observations of the discharge activity that leads to M-components. The relevant findings obtained from the images of high-speed video and interferometer (INTF) reveal that some typical M components are associated with positive streamers, fast negative streamers, or the interception of separate in-cloud leaders (Flache et al., 2008; Mazur et al., 1995; Mazur & Ruhnke, 2011; Shao et al., 1995; Yoshida et al., 2012). But it is not yet clear what discharge processes lead to M components having large peak currents. Up to now, there is no widely accepted conclusion on the initiation of large M components.

To better understand the initiation of large M components, we thoroughly analyze the current characteristics of M components and the related discharge processes based on channel-base current data, high-speed video observations, and the radiation source locations of flash-continuous INTF observations acquired from lightning flashes triggered in Guangdong province of China from 2014 to 2016. Considering that *M component* only depicts the stage of clearly detectable current change, we use *M event* to describe the processes, including the measured M current and the discharge processes leading to the current.

2. Experimental Equipment and Data

In this study, 239 M components during 18 triggered lightning flashes are analyzed. The channel-base current, electric field change, and high-speed images were observed during Guangdong Comprehensive Observation Experiment on Lightning Discharge from 2014 to 2016. The experiment was jointly conducted by the Chinese Academy of Meteorological Sciences and the Guangdong Meteorological Bureau at the *Guangzhou Field Experiment Site for Lightning Research and Testing* in the Conghua district, Guangdong province since 2006. The layout of the experimental instrument is shown in Figure 1.

The radiation sources of three triggered lightning flashes were located by a flash-continuous very high frequency (VHF) INTF that was installed in 2016 at a site of \sim 90-m distance from the rocket launcher. The INTF consisted of three broadband VHF antennas placed at the vertices of an equilateral triangle 20 m on each side. The signals from each of these VHF antennas were band-pass filtered to 25–90 MHz and recorded continuously with 16-bit resolution and sampling rate of 200 MHz for 2 s. The recorded waveforms were post-processed utilizing generalized cross-correlation time delay algorithm (Stock et al., 2014; Sun et al., 2013), applied to sequences of overlapping data segments from the time series waveforms. Additional information on the INTF is presented by Zhang et al. (2017). The propagation velocity of the VHF radiation sources is estimated in the same manner as in Shao et al. (1995), except that the discharge altitudes are better determined from lightning LF electric field detection array (LFEDA) data. The LFEDA, developed by Yang Zhang and Dong Zheng in 2015, locates the sources of LF discharge pulses in 3-D and time. Detailed information about LFEDA has been presented by Shi et al. (2017).

Channel-base current was measured by a coaxial shunt having a resistance of 1 m Ω and an upper frequency response of 200 MHz. The shunt was placed at the bottom of a lightning rod located in the middle of rocket launcher, and the current waveform was digitized by an isolated digitizer (HBM HV6600). After

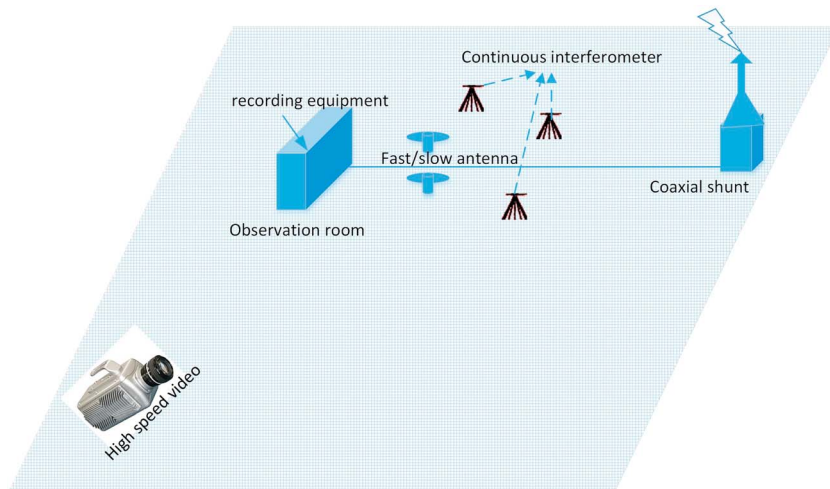


Figure 1. Layout of the experimental instrument in experiment field.

being transmitted via optical fiber to a remote transient recorder (HBM GEN5i), the current data were recorded for two channels with small (usually ± 2 kA) and large (usually ± 50 kA) measurement ranges. Also, the ± 2 kA current was separately digitized and recorded in synchronization with the INTF data. Detailed information about the current measurement system can be found in the studies by Zhang et al. (2016, 2017). A positive current value corresponds to negative charge moving downward or positive charge moving upward.

Electric field change (E) signals were measured by a capacitively coupled, flat-plate sensor (often called fast/slow antennas) installed flush with ground and located 80 m north of the launcher tower. The decay time constants of the fast/slow antennas were 2 ms and 4 s, respectively. The corresponding frequency bandwidths were ~ 80 Hz to 2 MHz and 0.04 Hz to 2 MHz. The signals were digitized at a sample rate of 10 MHz and recorded using a DL750 digitizer. Detailed information concerning the fast/slow antennas has been presented in the studies of Zhang et al. (2013, 2015). We use the atmospheric sign convention for electric fields, namely that the addition of positive charge overhead (or equivalently, the removal of negative charge) produces a positive E field change at the ground. The high-speed video images were obtained from a MotionPro HS-4 camera, located 1,900 m away from the rocket launcher. It recorded the triggered lightning flashes with a frame rate of 5000 fps and 512×512 pixels, corresponding to a spatial resolution of about 6 m above the launch tower.

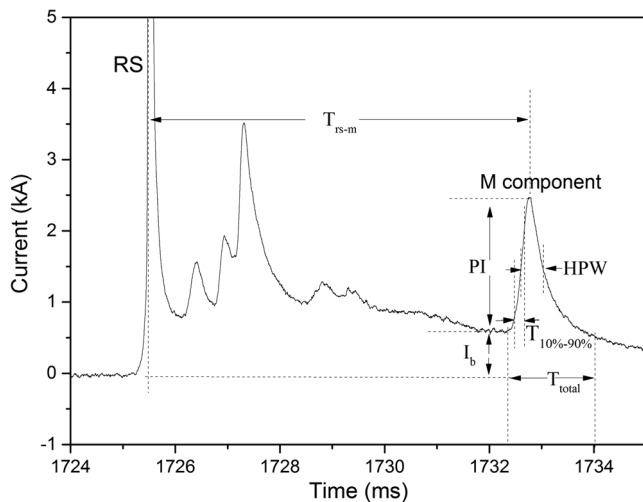


Figure 2. Graphical parameters of PI, T_{total} , $T_{10-90\%}$, HPW, T_{rs-m} , and I_b . RS = return stroke; T_{rs-m} = interval from return stroke to M; PI = peak current; HPW = half peak width; I_b = background current; $T_{10-90\%}$ = rise time from 10% to 90% peak; T_{total} = duration.

3. Results

3.1. Correlations Between the Current Parameters of M Events

Based on the analysis of current waveforms of the 239 M events, the parameters including relative peak current (PI), duration (T_{total}), rise time from 10% to 90% peak ($T_{10-90\%}$), HPW, charge transfer (MQ), interval from RS to M (T_{rs-m}), and background current (I_b) were determined, and the correlations between peak current, background current, and other parameters were investigated. The parameters are shown graphically in Figure 2. The definitions of the parameters, including PI, T_{total} , $T_{10-90\%}$, HPW, and MQ are similar to those of Zhang et al. (2016) and Qie et al. (2011). PI is defined as the difference between the maximum value of the current pulse and the background current level. T_{total} is the time interval from the beginning of the wavefront to the end position at which the trailing edge of the current pulse becomes indistinguishable from the overall continuous current waveform. $T_{10-90\%}$ is the time interval on the wavefront between the

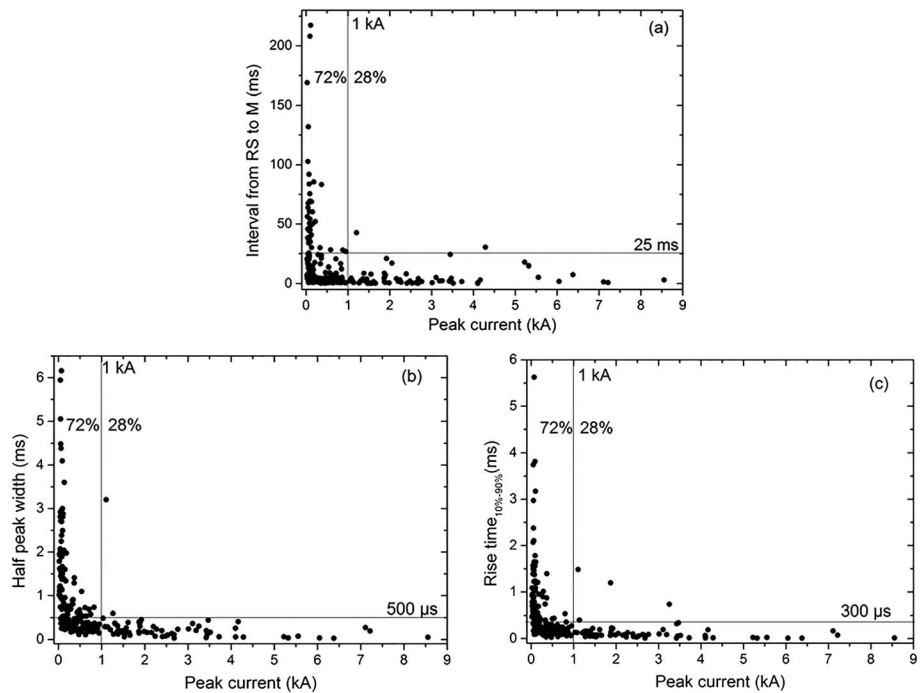


Figure 3. Correlations between the parameters of M components: (a) peak current versus interval from RS to M, (b) peak current versus half peak width, and (c) peak current versus rise time. RS = return stroke.

10% and 90% values of the peak value. HPW is the time interval between 50% values of the peak on the wavefront and on the falling portion of the event waveform. MQ is the time integral of the M current within the duration T_{total} . $T_{\text{rs-m}}$ is the time interval from the current peak of RS to the current peak of M event. The background current level (I_b) is the current value prior to a M current pulse, which provides an indication of the channel condition leading up to the M-component.

As can be seen in Figure 3, the peak currents of M events are related to the time interval between the RS to M event, as well as to the rise time (10–90%) and the HPW. A clearly visible *forbidden zone* (large upper right area) is a main characteristic of the correlation. Essentially, the M events with peak currents >1 kA occurred within 25 ms of the associated RS, rise times less than 300 μs and HPWs less than 500 μs . Although these boundaries are not absolute, the forbidden zone phenomenon is a clear feature of the observations. Similar correlations with the background current and $T_{\text{rs-m}}$, $T_{10-90\%}$ and HPW are also seen in Figure 4. When the background current is larger than 500 A, most of $T_{10-90\%}$ rise times are less than 300 μs and all RS–M intervals are less than 25 ms. Considering that the background current is associated with channel condition, it can be concluded that the channel condition prior to the M event is crucial to M current characteristics. The forbidden zone correlations reveal that the M events with large peak current and large background current occur often closer (in time) to RS, and have faster rise time and narrower HPW. At the same time, it can be seen that many M events having peak currents less than 1 kA and background currents less than 500 A also have the characteristics of fast rise time, short RS–M interval, and narrow HPW.

Some large current M events (RM type) were mentioned by Qie et al. (2011). Although there was no direct evidence of channel images in the video, they reasonably speculated on the discharge processes of large M events based on simultaneous electric field and current waveforms. In particular, they proposed that RM events correspond to the simultaneous presence of a dart leader and M incident wave in the channel. Two channel branches with overlapping lower portions coexist simultaneously in the upper part of the discharge channel. The continuing current flows in one branch while a leader–RS sequence propagates along the other branch. In order to better understand the discharge processes leading to M events with large current, we will show VHF radiation source observations and high-speed images in section 3.3.

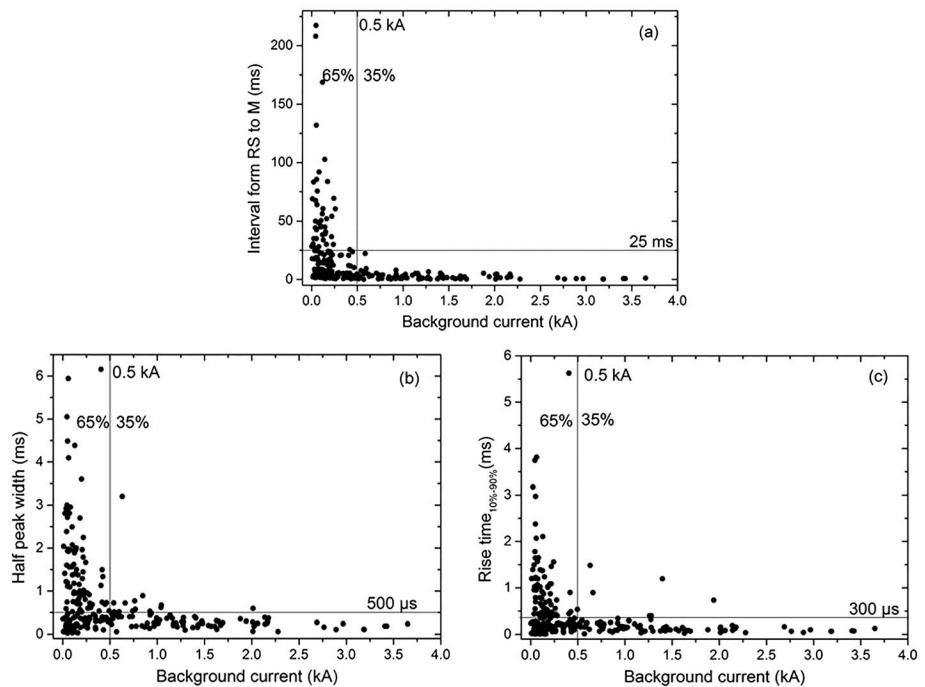


Figure 4. Correlations between the parameters of M components: (a) background current versus interval from RS to M, (b) background current versus half peak width, and (c) background current versus rise time. RS = return stroke.

3.2. Current Characteristics of M Events Having Large Peak Current

Of the 239 events studied here, 68 (28%) had peak currents exceeding 1 kA. The percentage of large current M components was also studied by Jiang et al. (2013). They found 11 out of 63 M events had currents exceeding 1 kA. Table 1 shows the parameters of the M events with large peak current from the present study. The geometric mean of peak current, duration, rise time from 10% to 90%, HPW, charge transfer, interval from RS to M, and background current were 2.358 kA, 0.627 ms, 0.078 ms, 0.165 ms, 0.417 C, 2.172 ms, and 579 A, respectively. In contrast, the corresponding values of lower-current M events were 197 A, 1.683 ms, 0.33 ms, 0.646 ms, 0.128 C, 7.175 ms, and 233 A, respectively (Table 2). Compared with the large M events, the weaker M events had lower peak current, longer duration, slower rise time, wider HPW, less charge transfer, longer interval from RS to M, and lower background current. Most of the parameters of large M events are similar to the results of Jiang et al. (2013). Their study showed that the peak current, duration, rise time, HPW, and charge transfer were 2.74 kA, 0.65 ms, 57 μs, 59 μs, and 0.353 C, respectively.

Table 1
Parameters of the Large 68 M Events

Parameter type/unit	Max	Min	GM
PI/kA	8.555	1.037	2.358
T_{total} /ms	7.834	0.139	0.627
$T_{10-90\%}$ /ms	1.482	0.0076	0.078
HPW/ms	3.201	0.025	0.165
MQ/C	3.110	0.027	0.417
T_{rs-m} /ms	42.610	0.156	2.172
I_b /kA	3.650	0.008	0.579

Note. GM = geometric mean; PI = peak current; T_{total} = duration; $T_{10-90\%}$ = rise time from 10% to 90% peak; HPW = half peak width; MQ = charge transfer; T_{rs-m} = interval from return stroke to M; I_b = background current.

3.3. Three Examples of M Events Having Large Peak Currents

3.3.1. Discharge Processes for Large Peak Current Events M1 and M2

Figure 5 shows INTF observations and channel-base current of a triggered negative CG lightning discharge that was produced on 9 June 2016. The initial stroke occurred ~900 ms into the record and was followed by four subsequent strokes after ~1,400 ms in the record. Two M events having large peak currents (M1 and M2) occurred during the first and fourth subsequent RSs, as described in this section. As can be seen from Figures 5b and 5c, the strokes went to ground immediately east-south-east of the INTF, from high elevation angle to the south and southwest of the triggering site.

Figure 6 shows 4 ms of observations for the RS at 1,468 ms (called RS1), and its associated large M event, M1. Figure 6a shows the electric field change and channel-base current, while Figures 6b–6d show the

Table 2
Parameters of the Weak 171 M Events

Parameter type/unit	Max	Min	GM
PI/kA	0.954	0.022	0.197
T _{total} /ms	13.967	0.185	1.683
T _{10–90%} /ms	5.623	0.026	0.330
HPW/ms	6.154	0.107	0.646
MQ/C	0.796	0.016	0.128
T _{rs–m} /ms	217.316	0.339	7.175
I _b /kA	3.428	0.003	0.233

Note. GM = geometric mean; PI = peak current; T_{total} = duration; T_{10–90%} = rise time from 10% to 90% peak; HPW = half peak width; MQ = charge transfer; T_{rs–m} = interval from return stroke to M; I_b = background current.

corresponding INTF data. From the channel-base current waveform, M1 had a peak current of 1.69 kA; a preceding background current of 1.48 kA; a transfer charge of 0.48 C; and 10%–90% rise time, HPW, and RS–M interval of 0.108 ms, 0.242 ms, and 0.757 ms, respectively.

Figures 6b–6d show the VHF radiation sources during the dart leader prior to the RS and following the RS leading up to M1. The leader developed along a complex path inside the storm before turning downward to ground (labeled as C1), making contact with the triggering wire triggering channel at ~1,468 ms. About 250 μs into the ensuing return stroke, fast breakdown began at a sharp bend (*kink*) in the leader channel and propagated horizontally away from the channel along a path not previously traversed by the flash (labeled C2). The radiation sources propagated an estimated 3.9 km distance in ~190 μs, corresponding to a 2-D speed of 2.1×10^7 m/s. Because its motion was mostly transverse to

the propagation direction from the observing site, its electric field change was minimal (E change P1), but the direction of propagation was clearly that of positive breakdown. The large channel-base current of M1 began about 150 μs later (E change P2), indicative of negative charge flowing to ground.

The above observations are fully consistent with those reported by Shao et al. (1995), in which fast positive breakdown (FPB) was also observed to develop away from channel kinks and led to an M event down to ground. Their observations showed the M event was initiated by an even faster *recoil* event back along the path of the fast breakdown, which continued on to ground as a dart leader. In several cases, the recoil breakdown was seen by their INTF and propagated at estimated speeds as high as $1\text{--}2 \times 10^8$ m/s. In other cases, occurrence of the recoil event was inferred by rejuvenation of the fast E change data. That is also the case for M1 of the present study, not only in the fast E data of Figure 6a, but also in the channel-base current, which was not available for the observations of Shao et al. (1995). The channel-base current measurement that is an advantage of triggered lightning observations provides clear proof of the recoil's occurrence.

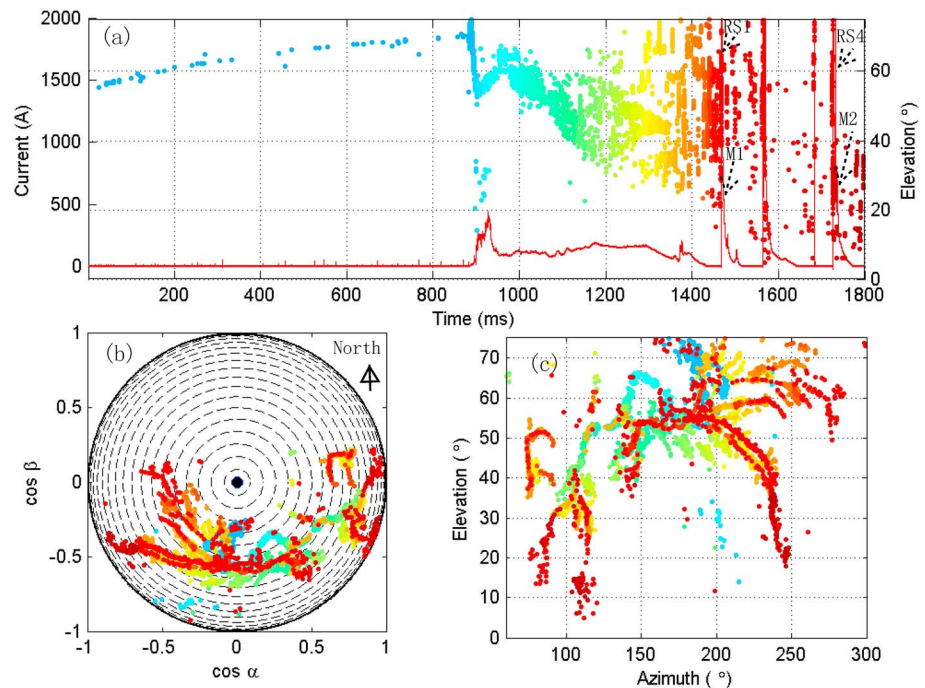


Figure 5. Radiation sources distribution and channel-base current of the triggered discharge on 9 June 2016: (a) radiation sources and channel-base current versus time; (b) hemispherical projection of radiation sources; (c) elevation of radiation sources versus azimuth. Colors from blue to red correspond to increasing time. RS = return stroke.

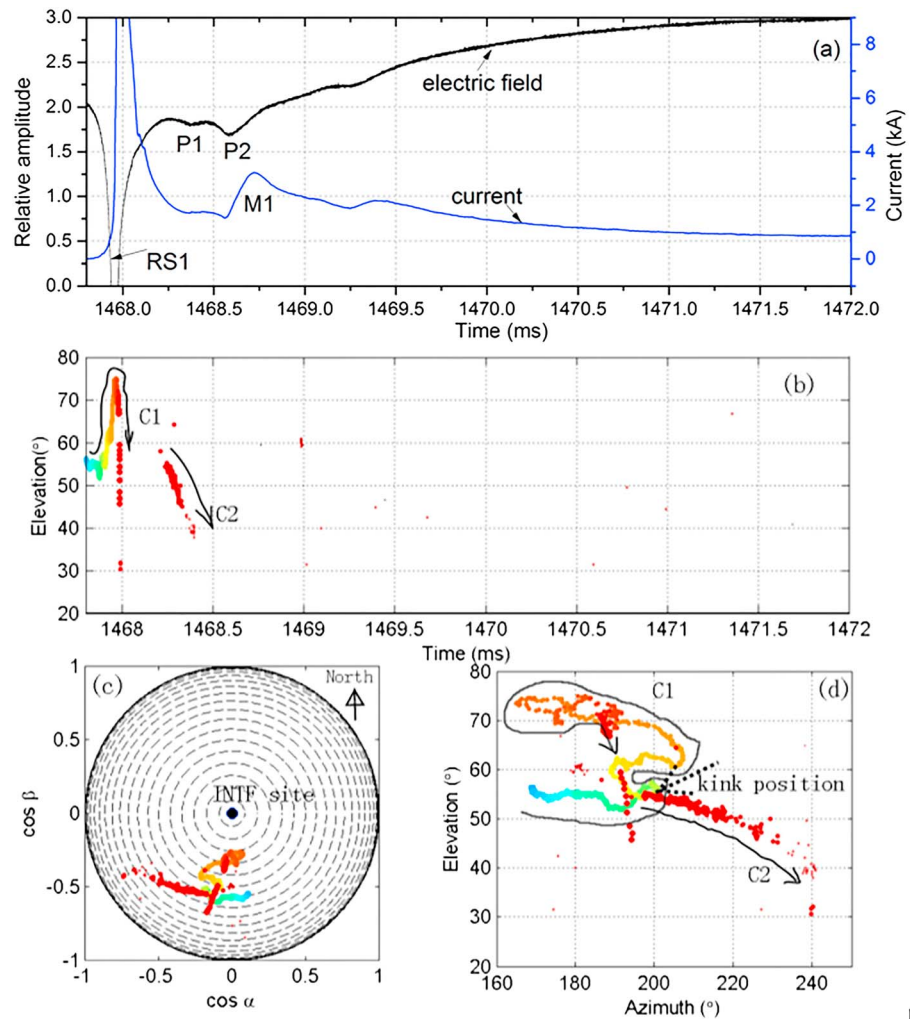


Figure 6. Radiation sources distribution, channel-base current, and the corresponding electric field of M1: (a) waveforms of electric field and channel-base current versus time, P1: the first electric field pulse, P2: the second electric field pulse, M1: M component 1; (b) elevation of radiation sources versus time; (c) hemispherical projection of radiation sources; (d) elevation of radiation sources versus azimuth. Colors of the radiation sources from blue to red correspond to increasing time in (b)–(d). C1 indicates the leader path, C2 indicates the forward propagation of M1. RS = return stroke.

Recent observations with a forerunner of the present INTF (Rison et al., 2016) show that high power narrow bipolar events (NBEs) are also produced by FPB. Although the NBE breakdown occurs in completely virgin air at the very beginning of flashes (Rison et al., 2016), the FPB of NBEs was noted to be the same as that of the M events of Shao et al. (1995). The identical nature of NBE-FPB (FPB of NBEs) and M-FPB (FPB of M events) is further confirmed by the observations of the present study.

Event M2 occurred after the fourth subsequent RS during the same triggered flash. Figure 7 shows the waveforms and INTF observations for this event, in the same format as Figure 6. In this case, the M event occurred ~ 7 ms after the RS, but still during the extended continuing current phase of the stroke. It was preceded by three M events within ~ 2 ms of the post-RS interval that produced significant channel-base currents, but were further away from the INTF and not as well detected by the INTF. As seen in Figure 7b, M2 was produced by a clear FPB event followed by an even faster negative recoil (labeled C2 and C3, respectively). The ensuing leader to ground was not detected by the INTF, but its occurrence is clearly shown by the channel-base current waveform (Figure 7a).

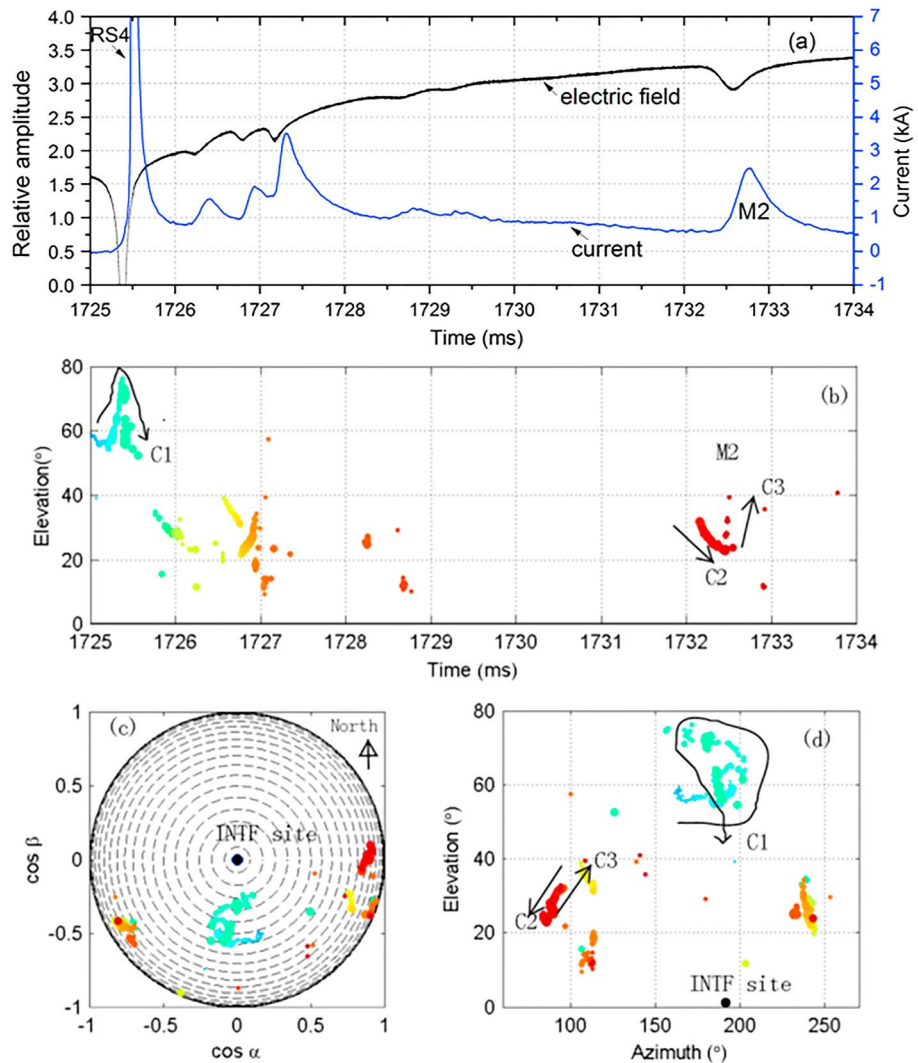


Figure 7. Radiation sources distribution, channel-base current, and the corresponding electric field of M2: (a) waveforms of electric field and channel-base current versus time; (b) elevation of radiation sources versus time; (c) hemispherical projection of radiation sources; (d) elevation of radiation sources versus azimuth. Colors of the radiation sources from blue to red correspond to increasing time in (b)–(d). C1 indicates the leader path, C2 indicates the forward propagation of M2, C3 indicates the recoil event of M2. RS = return stroke; INIF = interferometer.

The FPB (C2) propagated an estimated distance of 2.6 km in 280 μ s, corresponding to a 2-D velocity of 0.93×10^7 m/s. The recoil event had an estimated speed of 6.3×10^7 m/s. The resulting channel-base waveform had a peak current of 1.96 kA; a preceding background current of 0.51 kA; a charge transfer of 0.91 C; and 10%–90% rise time, HPW, and RS-M interval of 0.221, 0.396, and 7.283 ms, respectively. As seen for M1, M2 kept the continuing current alive. The observations agree perfectly with those obtained by Shao et al. (1995) and expand upon them by showing the channel-base current, thereby providing a quantitative measure of the M-event’s strength.

The M activity during the first 2 ms following RS4 occurred at the far southwest end of the lightning channel (lower left hand corner of Figure 7c). Although more distant, its limited INIF data showed evidence of FPB associated with at least one of the early M events. By contrast, M2 occurred on the right hand side of Figure 7c. All four of the M events occurred during a long continuing current that was originating in the southwest and were detected by the channel-base current. The channel of the continuing current probably remained conducting at the time of M2 and provided a conducting path from its FPB and recoil to the ground. Thus, M2 was somewhat similar to the hybrid RM event of the study by Qie et al. (2011), in that it occurred along a branch that connected into a path in common with the continuing current.

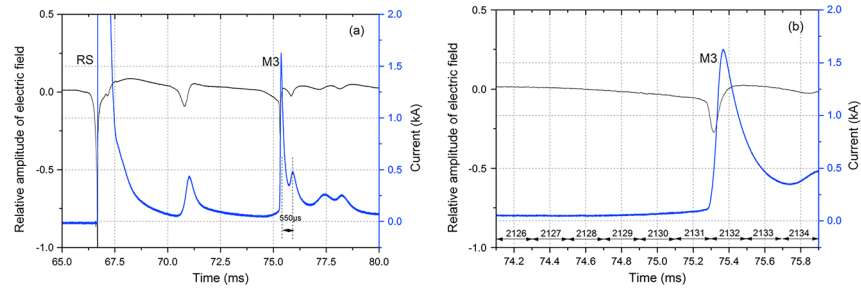


Figure 8. (a) Waveforms of current, electric field during the third RS and (b) expanded waveforms during M3 stage. The numbers in (b) correspond to of the frame indices of the high-speed video images. RS = return stroke.

3.3.2. Discharge Processes for Large Peak Current Event M3

A multistroke negative triggered lightning including 12 RSs was observed by high-speed video, slow antenna, and current measurement apparatus on 20 June 2014 when the INTF was not yet operational. Figure 8 shows the current and electric field waveforms for the third RS. A large M event (M3) occurred ~ 8.5 ms after the RS. It had a peak current of 1.51 kA; a background current of 0.11 kA; a transfer charge of 0.23 C; and 10–90% rise time, HPW, and RS-M interval of 0.049, 0.124, and 8.5 ms, respectively. Compared with M1 and M2, the current pulse of M3 was relatively narrow. Its channel-base current occurred almost simultaneously with its electric field change, similar to that of high building lightning shown in Figure 11 of Zhou et al. (2015). Furthermore, a subpulse can be found on the falling edge of the first pulse of M3 current from Figure 8a. The current waveform of M3 had two peaks, similar to the RM type described by Qie et al. (2011), but the interval between the two peaks was ~ 550 μ s, far too long for this event to be of RM type, for which the typical interval between peaks was 27.2 μ s in the study of Qie et al. (2011). Instead, comparison with electric field waveform indicates that the secondary current pulse was produced by a separate M event.

Figure 9 shows the images of channel path during the initial continuous current (ICC) and the third RS of the flash. Although it is difficult to see in the underexposed and overexposed pair of images, careful examination showed that the third RS (Figure 9b) developed along one of the two branches (Figure 9a) generated during the ICC stage. Figure 10 shows the images of discharge channel during M3. M3's discharge channel followed a path generated during ICC, seen faintly to the left of the *old path* in Figure 9a, while the channel of M3's parent RS (the third RS) still existed by the time of M3 but had weak luminosity. The sequence of photos in Figure 10 shows that M3 developed at an estimated 2-D speed of about 10^6 m/s down to the third RS path and contacted with the lower portion P1 of the third RS path in Frame 2131. The contact's occurrence coincided with the M3 electric field pulse (Figure 8), followed shortly afterward by the rapid channel-base current increase. Contact with the ground and the resulting propagation of ground potential up to the M3 channel caused renewed brightening and elongation of its upper channel, seen in the images 2132–2134 of Figure 10.

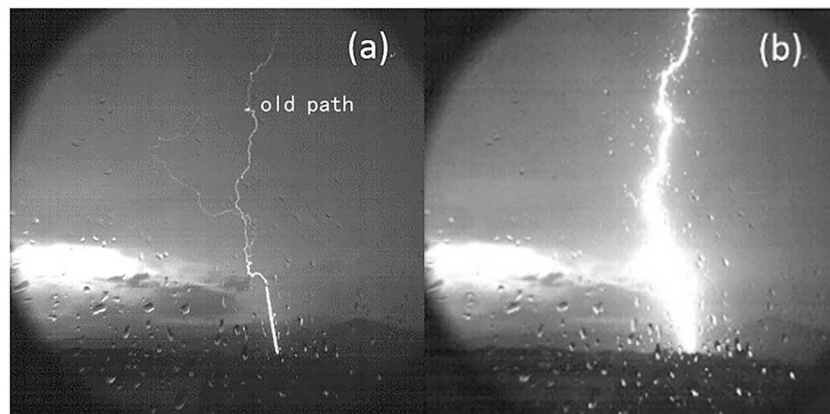


Figure 9. (a) Channel images during initial continuous current and (b) the third return stroke.

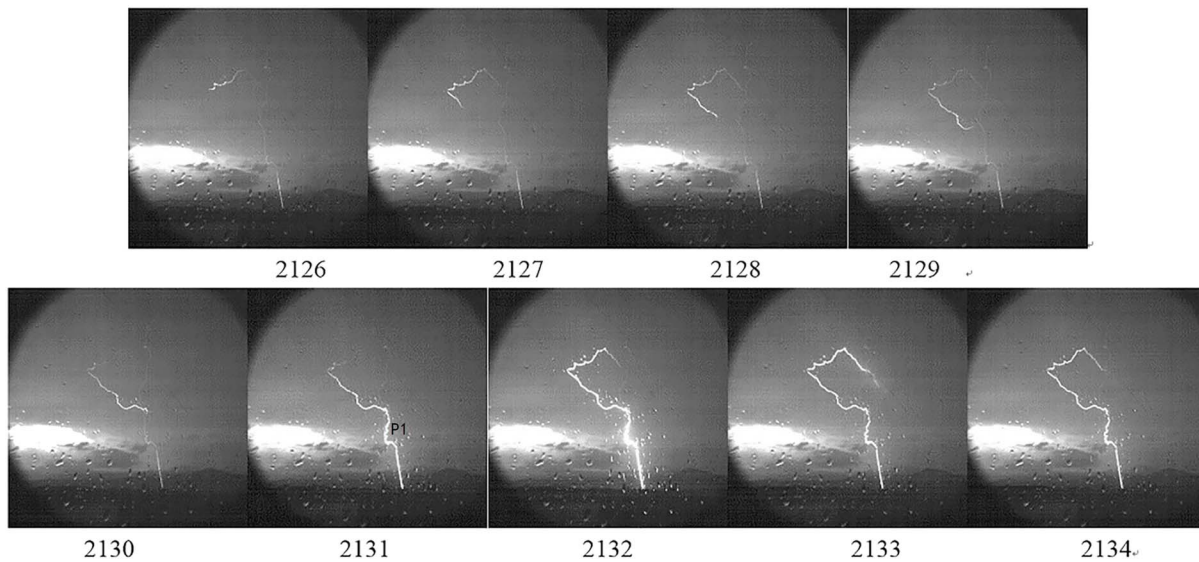


Figure 10. Channel images during M3 (frames from 2126 to 2134). The number below each image is the index of each frame.

We refer to this complex charge transferring mode as a mixed mode mentioned by Zhou et al. (2015). The mixed mode is characterized by two concurrent charge transfer processes: the downward leader/RS and weak continuing current of the parent RS, and the new discharge activity in a decayed branch produced during the ICC, with the connection point being at low altitude, leading to a characteristically narrow current pulse.

4. Discussion and Conclusions

Based on the data of channel-base current, electric field change, high-speed images, and radiation sources locations, 239 M events during 18 triggered lightning flashes were investigated. The current characteristics and the correlations between the current parameters of M events are presented. In addition, the discharge processes leading to large M-event currents are shown in detail. The detailed results are as follows.

Sixty-eight of all 239 M events (28%) involve peak currents exceeding 1 kA. Their geometric average values of peak current, duration, 10–90% rise time, HPW, charge transfer, interval from RS to M, and background current were 2.358 kA, 0.627 ms, 0.078 ms, 0.165 ms, 0.417 C, 2.172 ms, and 579 A, respectively. The peak current and background current of the M events are found to be related to their 10–90% rise time, HPW, and interval from RS to M. A forbidden zone in the correlation between the current parameters has been observed. Compared to the regular, lower-current M events, M events with large current often occur closer in time to the parent RS, and have faster rise times, narrower HPWs, and larger charge transfers. If we use *fast* or *slow* to describe the type of pulse current, similar to Flache et al. (2008), the large M current would correspond to a fast M event. The results are similar to the ICC pulse mentioned by Flache et al. (2008). They reported that all of the fast ICC pulses have large peak currents, ranging from 3.6 to 13 kA. But as mentioned in section 3.1, some fast M current pulses are also associated with small M currents, although all large M events correspond to sharp M current. This indicates that a fast current pulse is a necessary, but not sufficient, condition for the occurrence of large M currents.

The cases of M1 and M2 reveal that some of the large M events are caused by fast positive streamers followed by observed or inferred recoil event. The fast positive streamers propagate away from the RS channel at a velocity of $\sim 10^7$ m/s and produce a recoil event back along the positive streamer path into the conducting channel and to ground. This is fully consistent with the observations of Shao et al. (1995). Considering the existence of long conductive channel during the above discharge, M1 and M2 transported charge by a classical M-component mode. Both the forward positive streamers and the following recoil event can contribute to the large M current. The current changes began during the discharge process of the positive streamers, which indicates that the positive streamers might be an important factor in determining the large M

current. The relevant effect will be investigated in later work. Although both M1 and M2 were initiated by fast positive streamers, there was no clearly visible radiation sources of recoil event to be located for M1. Compared to the current parameters of M2, M1 has larger background current (1.483 vs. 0.51 kA). The large background current has to do with a large electric potential difference and good channel condition, which maybe lead to the absence of radiation sources.

The case of M3 indicates that some of the large M events are associated with downward leader/upward RS sequences in one branch while another branch is carrying a continuing current. The two branches have a common channel section attached to ground. M3 transported charge by a mixed mode after connection, which led to fast current change. Due to the absence of an in-cloud discharge channel for M3, we cannot tell whether a positive streamer or recoil event similar to M1 and M2 has occurred. However, considering the insignificant current change during the downward development, we speculate that the downward negative leader occurs indeed in a separate channel. The separate leader usually carries a lot of charge, which often causes large current change. Although the path of the downward M3 leader was not the same as that of the preceding dart leader, its path was the same as one of the ICC pulses (Figure 9a). Therefore, we consider that the downward leader of M3 could be a dart leader.

Compared with the visible junction of M3 in the high-speed images, the junction of M1 cannot be observed by the same high-speed video, which indicates that the junction position of M3 is lower than that of M1. At the same time, the radiation source locations reveal that M1 is closer to the main grounding channel than M2. Therefore, the order of junction position is M2, M1, and M3 from far to near, while the corresponding rise times of M currents are 0.221, 0.108, and 0.049 ms, respectively. This indicates that the rise time of the M-current pulse is related to the junction position. The sharper current pulse corresponds to a lower/closer junction position, which might be due to a shorter propagation path from connection position to ground. Considering that the *classical* M-component mode often corresponds to slow M-current pulse, we agree with the opinion that classical M-component mode is not possible in the case of a low junction point (Zhou et al., 2015).

Acknowledgments

This research is funded by the National Natural Science Foundation of China (41775009, 91537209), the National Key Research and Development Program of China (2017YFC1501501), the National Key Basic Research Program of China (2014CB441405, 2014CB441406), and the Basic Research Fund of Chinese Academy of Meteorological Sciences (Grant No.2018Z003). We are thankful to Paul R. Krehbiel for polishing the English language, ShaoDong Chen and Xu Yan for the assistance in experimental maintenance. The data may be obtained from the shared network location (<https://pan.baidu.com/s/1wTd0dwJ9uzLMrdSSpsf7Kg>).

References

- Chen, S. D., Zhang, Y. J., Zhou, M., Yan, X., Lu, W. T., Chen, L. W., & Zhang, Y. (2018). Observation of residual voltage in low-voltage surge protective devices due to nearby M-components. *IEEE Transactions on Electromagnetic Compatibility*, *60*(3), 776–784. <https://doi.org/10.1109/TEMC.2017.2737648>
- Fisher, R. J., Schnetzer, G. H., Thottappillil, R., Rakov, V. A., Uman, M. A., & Goldberg, J. D. (1993). Parameters of triggered-lightning flashes in Florida and Alabama. *Journal of Geophysical Research*, *98*(D12), 22,887–22,902. <https://doi.org/10.1029/93JD02293>
- Flache, D., Rakov, V. A., Heidler, F., Zischank, W., & Thottappillil, R. (2008). Initial-stage pulses in upward lightning: Leader/return stroke versus M-component mode of charge transfer to ground. *Geophysical Research Letters*, *35*(13), L13812. <https://doi.org/10.1029/2008GL034148>
- Jiang, R., Qie, X., Wang, C., Yang, J., Zhang, Q., Wang, J., & Liu, D. (2011). Lightning M-components with peak current in the range of kilo amperes and their mechanism. *Acta Physica Sinica*, *60*(7), 867–874.
- Jiang, R., Qie, X., Yang, J., Wang, C., & Zhao, Y. (2013). Characteristics of M-component in rocket-triggered lightning and a discussion on its mechanism. *Radio Science*, *48*, 597–606. <https://doi.org/10.1002/rds.20065>
- Mazur, V., Krehbiel, P. R., & Shao, X. M. (1995). Correlated high-speed video and radio interferometric observations of a cloud-to-ground lightning flash. *Journal of Geophysical Research*, *100*(D12), 25,731–25,753. <https://doi.org/10.1029/95JD02364>
- Mazur, V., & Ruhnke, L. H. (2011). Physical processes during development of upward leaders from tall structures. *Journal of Electrostatics*, *69*(2), 97–110. <https://doi.org/10.1016/j.elstat.2011.01.003>
- Qie, X., Jiang, R., Wang, C., Yang, J., Wang, J., & Liu, D. (2011). Simultaneously measured current, luminosity, and electric field pulses in a rocket-triggered lightning flash. *Journal of Geophysical Research*, *116*, D10102. <https://doi.org/10.1029/2010JD015331>
- Qie, X., Jiang, R., & Yang, J. (2013). Characteristics of current pulses in rocket-triggered lightning. *Atmospheric Research*, *135–136*, 322–329. <https://doi.org/10.1016/j.atmosres.2012.11.012>
- Rakov, V. A. (1998). Some inferences on the propagation mechanisms of dart leaders and return strokes. *Journal of Geophysical Research*, *103*(D2), 1879–1887. <https://doi.org/10.1029/97JD03116>
- Rakov, V. A., Crawford, D. E., Rambo, K. J., Schnetzer, G. H., Uman, M. A., & Thottappillil, R. (2001). M-component mode of charge transfer to ground in lightning discharges. *Journal of Geophysical Research*, *106*(D19), 22,817–22,831. <https://doi.org/10.1029/2000JD000243>
- Rakov, V. A., Thottappillil, R., Uman, M. A., & Barker, P. P. (1995). Mechanism of the lightning M component. *Journal of Geophysical Research*, *100*(D12), 25,701–25,710. <https://doi.org/10.1029/95JD01924>
- Rakov, V. A., & Uman, M. A. (2003). *Lightning: Physics and effects*. New York: Cambridge University Press. <https://doi.org/10.1017/CBO9781107340886>
- Rison, W., Krehbiel, P. R., Stock, M. G., Edens, H. E., Shao, X. M., Thomas, R. J., et al. (2016). Observations of narrow bipolar events reveal how lightning is initiated in thunderstorms. *Nature Communications*, *7*, 10,721. <https://doi.org/10.1038/ncomms10721>
- Shao, X. M., Krehbiel, P. R., Thomas, R. J., & Rison, W. (1995). Radio interferometric observations of cloud-to-ground lightning phenomena in Florida. *Journal of Geophysical Research*, *100*(D2), 2749–2783. <https://doi.org/10.1029/94JD01943>
- Shi, D. D., Zheng, D., Zhang, Y., Zhang, Y. J., Huang, Z. G., Lu, W. T., et al. (2017). Low-frequency E-field Detection Array (LFEDA)—Construction and preliminary results. *Science China: Earth Sciences*, *10*, 1–13.

- Stock, M. G., Akita, M., Krehbiel, P. R., Rison, W., Edens, H. E., Kawasaki, Z., & Stanley, M. A. (2014). Continuous broadband digital interferometry of lightning using a generalized cross-correlation algorithm. *Journal of Geophysical Research: Atmospheres*, *119*, 3134–3165. <https://doi.org/10.1002/2013JD020217>
- Sun, Z., Qie, X., Liu, M., Cao, D., & Wang, D. (2013). Lightning VHF radiation location system based on short-baseline TDOA technique—Validation in rocket-triggered lightning. *Atmospheric Research*, *129-130*, 58–66. <https://doi.org/10.1016/j.atmosres.2012.11.010>
- Thottappillil, R., Goldberg, J. D., Rakov, V. A., Uman, M. A., Fisher, R. J., & Schnetzer, G. H. (1995). Properties of M components from currents measured at triggered lightning channel base. *Journal of Geophysical Research*, *100(D12)*, 25,711–25,720. <https://doi.org/10.1029/95JD02734>
- Wang, C., Jiang, R., Yang, J., & Liu, M. (2012). Current subsidiary peak in triggered lightning strokes. *Radio Science*, *47*, RS4002. <https://doi.org/10.1029/2011RS004933>
- Wang, D., Takagi, N., & Watanabe, T. (2007). Observed characteristics of luminous variation events during the of luminous variation events during the initial state of upward positive leaders. *Journal of the Atmospheric Electricity*, *7(1)*, 61–68.
- Yoshida, S., Biagi, C. J., Rakov, V. A., Hill, J. D., Stapleton, M. V., Jordan, D. M., et al. (2012). The initial stage processes of rocket-and-wire triggered lightning as observed by VHF interferometry. *Journal of Geophysical Research*, *117(D9)*, D09119. <https://doi.org/10.1029/2012JD017657>
- Zhang, Y., Krehbiel, P. R., Zhang, Y., Lu, W., Zheng, D., Xu, L., & Huang, Z. (2017). Observations of the initial stage of a rocket-and-wire-triggered lightning discharge. *Geophysical Research Letters*, *44*, 4332–4340. <https://doi.org/10.1002/2017GL072843>
- Zhang, Y., Zhang, Y. J., Lu, W. T., & Zheng, D. (2013). Analysis and comparison of initial breakdown pulses for positive cloud-to-ground flashes observed in Beijing and Guangzhou. *Atmospheric Research*, *129-130*, 34–41. <https://doi.org/10.1016/j.atmosres.2013.03.006>
- Zhang, Y., Zhang, Y. J., Xie, M., Zheng, D., Lu, W. T., Chen, S. D., & Yan, X. (2016). Characteristics and correlation of return stroke, M component and continuing current for triggered lightning. *Electric Power Systems Research*, *139*, 10–15. <https://doi.org/10.1016/j.epsr.2015.11.024>
- Zhang, Y., Zhang, Y. J., Zheng, D., & Lu, W. T. (2015). Preliminary breakdown, following lightning discharge processes and lower positive charge region. *Atmospheric Research*, *161-162*, 52–56. <https://doi.org/10.1016/j.atmosres.2015.03.017>
- Zhou, H. L., Rakov, V. A., Diendorfer, G., Thottappillil, R., Pichler, H., & Mair, M. (2015). A study of different modes of charge transfer to ground in upward lightning. *Journal of Atmospheric and Solar-Terrestrial Physics*, *125-126*, 38–49. <https://doi.org/10.1016/j.jastp.2015.02.008>